Self-Assembly of Bacteria in Alternating-Current Electric Fields

Yan-Ran Li(李艳冉)[1], Yi-Wu Zong(宗奕吾)[1*], Hong Zhang(张红)[2], Jing-Chao Zhang(张静超)[3], Chun-Ying Feng(冯春迎)[4,5], Jian-Jun Qiao(乔建军)[1,6], Hao Song(宋浩)[1,6], and Kun Zhao(赵坤)[7,8*]

[1]*Frontiers Science Center for Synthetic Biology and Key Laboratory of Systems Bioengineering (Ministry of Education), School of Chemical Engineering and Technology, Tianjin University, Tianjin 300072, China*
[2]*Petrochemical Research Institute of Petrochina Co., Ltd., Beijing 102206, China*
[3]*Center for Medical Genetics, Sichuan Provincial People's Hospital, University of Electronic Science and Technology of China, Chengdu 611731, China*
[4]*Jiangsu Key Laboratory of Sericultural and Animal Biotechnology, School of Biotechnology, Jiangsu University of Science and Technology, Zhenjiang 212100, China*
[5]*Key Laboratory of Silkworm and Mulberry Genetic Improvement, Ministry of Agriculture and Rural Affairs, Sericultural Scientific Research Center, Chinese Academy of Agricultural Sciences, Zhenjiang 212100, China*
[6]*Collaborative Innovation Center of Chemical Science and Engineering, Tianjin 300072, China*
[7]*The Sichuan Provincial Key Laboratory for Human Disease Gene Study and The Institute of Laboratory Medicine, Sichuan Provincial People's Hospital, University of Electronic Science and Technology of China, Chengdu 610054, China*
[8]*Institute of Fundamental and Frontier Sciences, University of Electronic Science and Technology of China, Chengdu 610054, China*

(Received 31 May 2024; accepted manuscript online 4 September 2024)

Self-assembly of bacteria in electric fields is a promising route to fabricate biomaterials with reversible and specific structures. However, due to relatively less studies, our understanding of the self-assembly of bacteria in electric fields is still incomplete. Particularly, how different bacterial species behave differently in their field-mediated self-assembly behavior remains to be disclosed. In this study, we choose four bacterial species, including *Shewanella oneidensis*, *Pseudomonas aeruginosa*, *Bacillus subtilis* and *Lactococcus lactis* as model systems, and investigate their self-assembly behavior in alternating-current (AC) electric fields for both diluted and concentrated suspensions. The phase diagrams in the plane of applied field strength vs frequency are obtained. The results show that in diluted suspensions, a transition sequence of isotropic–paranematic–string–columnar phases is observed in all strains as the field strength increases. Details of the assembled structures are quantitatively differentiated among different strains. In concentrated suspensions, besides the isotropic and paranematic phases, a higher ordered phase with interdigitating rectangular crystal domains (OIR) and an ordered phase with smectic A liquid crystal domains are observed for *S. oneidensis* and *P. aeruginosa*, respectively. Our findings shed new light on fabricating potential biomaterials by assembling cells of appropriately chosen bacterial species that have desired surface properties under AC electric fields.

DOI: 10.1088/0256-307X/41/10/108701

Self-assembly of nano/micro-sized matter is one of effective ways to construct functional materials with specific ordered structures.[1–7] Particularly, directed assembly mediated by external fields, such as electric[8–10] and/or magnetic[11,12] fields, has received a great deal of attention in recent years due to their advantages including non-contact manipulation, rapid response, and tunability. For example, the self-assembly of colloidal systems in alternating-current (AC) electric fields has been extensively studied, and different factors that can affect the assembled structures, such as particle shape,[13–15] interparticle interactions,[16] and polydispersity of the particles,[17] have been explored. Compared to non-living colloids, bacterial cells are unique in fabricating biomaterials.[18–23] They are alive so that they can grow and multiply.[24,25] Moreover, many bacterial species can also swim through rotations of flagella. Thus, in addition to the cell size, shape and polydispersity, the propulsion generated by flagella, as well as the complex chemical and physical properties of cells, in principle will also affect their assembly behavior in AC electric fields. With such a wide variety of parameters that can be manipulated, assembly of microbial cells in AC electric fields is expected to generate richer assembled structures and have great potentials in biomaterial applications. For instance, with the assistance of electric fields, tetrad clusters of *Micrococcus luteus* were shown to be able to assemble into double helix and bundles,[26] while fd virus could organize into various nematic phases.[19,22] Structures with higher orders were also reported. For example, *Salmonella typhimurium*

*Corresponding authors. Email: yiwuzong@tju.edu.cn; kzhao@uestc.edu.cn
© 2024 Chinese Physical Society and IOP Publishing Ltd

could form two-dimensional (2D) ordered arrays and three-dimensional (3D) columnar structures.[23] Despite these advances, compared with the extensive studies for the non-living counter parts, investigations on the self-assembly of bacteria in AC electric fields are still relatively less, which limits understandings of the underlying mechanisms and their further applications. Particularly, most previous studies including Refs. [23,26] have been focused on the assembling behavior of one type of strain, however, given that different bacterial species can vary greatly in cell morphology, cell surface properties as well as cell motility, how different bacterial species behave differently in their field-mediated self-assembly behavior remains to be disclosed.

In this work, we choose four bacterial species which are model organisms in both fundamental and applied biological studies, including two gram-negative species *Shewanella oneidensis* (*S. oneidensis*) and *Pseudomonas aeruginosa* (*P. aeruginosa*), and two gram-positive species *Bacillus subtilis* (*B. subtilis*) and *Lactococcus lactis* (*L. lactis*). Besides different cell structures, these four strains also vary in cell morphology and cell surface properties including shape, aspect ratio, zeta potential, and motility. For each species, to investigate cell assembly behavior in AC electric fields, we record the evolution of cell locations and orientations under certain applied AC electric field. The obtained recording data are then analyzed through bacterial tracking techniques, and the results are used to help determine the assembled structures. By varying the applied field strength and frequency, a phase diagram in the plane of field strength vs frequency is obtained. The self-assembly behavior of bacterial cells is studied in both diluted and concentrated suspensions. Our results reveal different assembly behaviors among the tested four species and are helpful for further understanding the role of cell morphology, cell surface properties, and cell motility in the field-mediated bacterial assembly.

Experimental Methods. The bacterial strains used in this study are *S. oneidensis* MR-1, *P. aeruginosa* PAO1, *B. subtilis* ATCC 6051, and *L. lactis* F44.[27] Cells of the four strains all have similar rod shapes, but their dispersed states are different. *S. oneidensis* and *P. aeruginosa* are dispersed as single cell suspensions. For *B. subtilis*, dimers or trimers of cells in suspensions can also be observed frequently, probably because of the effect of sticky exopolysaccharides produced by cells. *L. lactis* is quite different from other three strains as cells exist in pearl chain-like clusters consisting of different numbers of cells in each chain. The first three strains were cultured in Luria-Bertani broth [LB, tryptone 1% (w/v), yeast extract 0.5% (w/v), NaCl 1% (w/v)], in which *S. oneidensis* and *B. subtilis* were cultured overnight with shaking at 180 rpm and 30 ℃, while *P. aeruginosa* was incubated overnight with shaking at 37 ℃ and 220 rpm. For *L. lactis* strain, cells were cultured by standing overnight in M17 medium (Qingdao Hope Bio-Technology Co., Ltd.) with 0.5% glucose in an incubator at 30 ℃. To visualize the flagellum of a *P. aeruginosa* cell, a T394C mutation was engineered into the flagellum protein FliC to construct the mutant $\mathrm{FliC}^{\mathrm{T394C}}$ strain,[28] which can be labeled with Alexa Flour$^{\mathrm{TM}}$488 C5 Mal through 15-min incubating. Before injected into the sample cell, the bacteria suspensions were washed with deionized water by centrifugation for about 10 times, with each wash was performed at 5000 rpm for 2 min. The final obtained bacterial suspension after washing has a conductivity of 6.0 ± 1.5 μS/cm. The concentrations of the four bacterial suspensions are controlled by setting appropriate optical densities measured at 600 nm wavelength (OD_{600}). In this study, two concentrations of diluted ($\mathrm{OD}_{600} = 0.1$) and relatively concentrated ($\mathrm{OD}_{600} = 1.0$) suspensions were used.

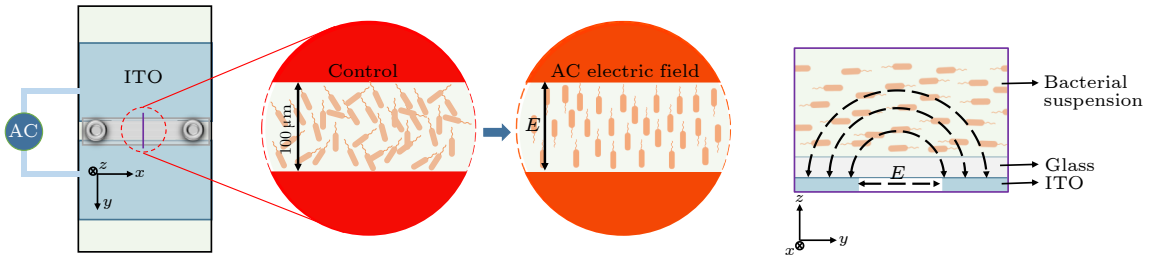

Fig. 1. Schematic of the experimental setup. Bacteria will align themselves along the direction of the electric field (y axis) when the field strength is above a threshold value. The graph on the right shows the side view of the setup, where dashed lines with double arrows indicate the non-uniform electric field generated by the two co-planar ITO electrodes.

The sample cell is constructed by an ibidi cell (Ibidi), which has a 17 mm × 3.8 mm × 0.4 mm channel. A cover glass (25 mm × 75 mm × 0.2 mm) containing two square regions (25 mm × 25 mm) with each being indium-tin-oxide (ITO) film coated is glued onto the bottom of the ibidi cell with the ITO coating side faced outwards, as is illustrated in Fig. 1. The two conducting ITO films are separated by a gap of $d = 100$ μm, and serve as two electrodes. Wires are attached to the ITO electrodes by conductive silver paste and will be connected to power sources. After injecting bacteria suspension into the sample cell, the two inlets of the sample cell are sealed by plugs. All exposed conductive components are sealed with ultraviolet curing optical adhesive (Norland 81) to form an insulating protective layer. The applied AC electric field is generated by a function generator (Tektronix AFG1022) coupled with a

power amplifier (Trek, PZD350A). A square wave of AC electric field was used. With the applied voltage $V(t)$,

$$V(t) = \begin{cases} V_{\rm a}^0, & nT \le t \le nT + \frac{T}{2}, \\ -V_{\rm a}^0, & nT + \frac{T}{2} \le t \le (n+1)T, \end{cases} \tag{1}$$

the amplitude of the applied electric field was calculated as $E_{\rm a}^0 = V_{\rm a}^0/d$. Here, $V_{\rm a}^0$ denotes the amplitude of applied voltage and $d = 100\,\mu$m. We note that the actual electric field strength in the suspensions will vary with the dielectric constant and conductivity of the suspension, as well as the frequency of the AC electric field.

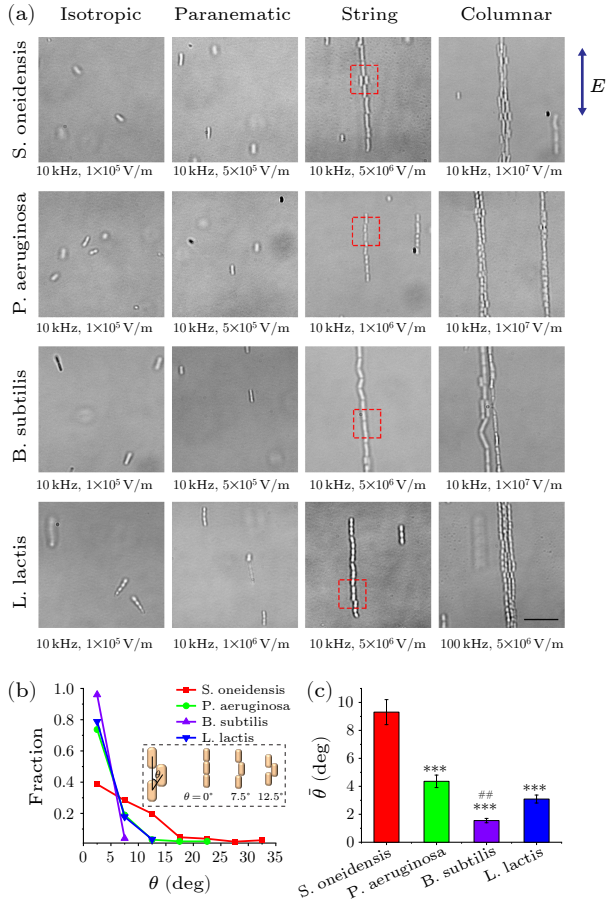

Fig. 2. (a) Typical microscopic images of different bacterial suspensions ($\rm OD_{600} = 0.1$) showing isotropic (first column), paranematic (second column), string (third column) and columnar (fourth column) phases. The two-headed arrow indicates the direction of the AC electric field. [(b), (c)] The distribution of θ (b) and its average value (c) obtained from string structures of four bacterial strains. The inset shown in the dashed rectangular box in (b) illustrates schematic diagrams of the definition of θ, and configurations with θ being 0°, 7.5°, and 12.5°, respectively. The total counting number of theta measurements is over 100. $^{***}p < 0.001$ indicates significant difference by ANOVA compared with *S. oneidensis*, while $^{\#\#}p < 0.01$ indicates significant difference by ANOVA compared with *P. aeruginosa*. Scale bar: 10 μm.

Microscopic images were captured by a point grey camera (FLIR) on a Leica DMi8 inverted microscope with a 100× oil objective lens, and subsequently were analyzed by user-written Matlab and interactive data language (IDL) codes with image processing algorithms in the same way as described in Refs. [29]. Fluorescence images (Fig. S4) were taken by a sCMOS camera (Prime 95B) on a Nikon Eclipse Ti2 inverted microscope.

Results. The self-assembly of dilute ($\rm OD_{600} = 0.1$) bacteria suspensions in AC electric fields were studied first. As shown in Fig. 2(a), when the voltage or frequency of the applied AC electric field increases, cells of all four species first transit from a randomly orientated isotropic phase to a paranematic phase in which cell orientations are aligned with the field direction, then orientated cells assemble into one-dimensional strings and finally into 3D columnar structures due to dipole-dipole interactions. Though all four species can form string and columnar structures, these structures of different species are distinguishable. For instance, taking string as an example [see examples outlined by red dashed boxes in Fig. 2(a)], *B. subtilis* cells tend to form a straight-line-like configuration with centers of cells are in a line, while *P. aeruginosa* and *L. lactis* cells tend to form a zig-zag-like line configuration with centers of neighboring cells being shifted laterally relative to the line axis, which thus demonstrate a small amount of misalignment of center-center directions of nearest neighboring cells from the electric field direction. In contrast to the aforementioned three species, *S. oneidensis* cells tend not to be head-tail aligned but rather to form a staggered-like string with two neighboring cells along the chain are completely offset laterally by one cell width. With such tendency, it is often observed that two parallel *S. oneidensis* cells can occupy the same string position with their orientations both aligned with the electric field. To quantitatively evaluate the differences in the string-like structures, we introduce an angle θ defined as the angle between two center-center lines (one is the center-center line connecting one cell with its nearest neighbor and the other is the one connecting the cell with its next nearest neighbor found along the same direction of the string), which is illustrated in Fig. 2(b) inset. Figures 2(b) and 2(c) show the measured distributions of θ and averaged values $\overline{\theta}$ for tested strains. For *B.* subtilis, θ has a relatively narrow distribution with the majority ($\sim 95\%$) located near 0°, suggesting that centers of cells in the string form a straight line; For *P. aeruginosa* and *L. lactis*, their θ distributions are both relatively wider than *B. subtilis* with a lower percentage ($\sim 78\%$) of θ near 0°. The percentage of $\theta \sim 7.5°$ increases considerably in these two strains, consistent with the more zig-zag-like configurations found in strings. As for *S. oneidensis*, the θ distribution is further widened, and the percentage for θ near 0° drops to 39% while the percentages for $\theta \sim 7.5°$ and $\theta \sim 12.5°$ increase to 28% and 20%, respectively. $\theta \sim 12.5°$ corresponds to the staggered-like configuration of neighboring cells [Fig. 2(b) inset]. Thus, the θ distribution of *S. oneidensis* clearly shows a different string structure from the others. This is also supported by $\overline{\theta}$ shown in Fig. 2(c), where $\overline{\theta}$ is $1.6° \pm 0.2°$ for *B. subtilis*, $4.4° \pm 0.4°$ for *P. aeruginosa*, $3.1° \pm 0.3°$ for *L. lactis*, and $9.3° \pm 0.9°$ for *S. oneidensis*. It has been shown that isotropic particles

could assemble into perfect linear structures in AC electric field,[30,31] while the anisotropic particles tend to form imperfect linear string structure[15,32] with $\theta > 0$. In literature it is also suggested that θ is related to the aspect ratio of bacteria.[23] In our experiments, the aspect ratios of *B. subtilis* and *S. oneidensis* are 7.0 ± 0.6 and 6.1 ± 0.6, respectively (see Fig. S1 in the Supplementary Materials), while their string structures vary greatly. *P. aeruginosa* and *L. lactis* have smaller aspect ratios, which are 3.5 ± 0.3 and 2.1 ± 0.2, respectively, but their θ values are in between *B. subtilis* and *S. oneidensis*. Together, our experimental observations suggest that the aspect ratio of bacteria can affect the final string structures but the relationship is complex. It is worth pointing out that the aspect ratio of *L. lactis* is referred to the aspect ratio of a single rod-like unit cell, instead the whole pearl chain-like cluster.

By varying the field strength and frequency, we can get a phase diagram of the diluted suspension ($OD_{600} = 0.1$) in AC electric fields for each species (Fig. 3). To quantitatively differentiate the paranematic phase from the isotropic phase, we calculated the nematic order parameter $\Phi_2 = N^{-1}|\sum_{j=1}^{N} e^{i2\gamma_j}|$. Here, γ_j denotes the orientational angle of cell j, and N is the number of bacterial cells. The systems with $\Phi_2 > 0.6$ are classified into paranematic phases. For string phases, a string is defined as a chaining cluster consisting of ≥ 5 cells. As shown in Fig. 3, at a small fixed frequency $f = 10\,\text{Hz}$, the threshold value of applied electric field necessary to align *S. oneidensis* or *B. subtilis* is markedly lower than those for *P. aeruginosa* and *L. lactis* as the latter two strains do not show paranematic phase within the tested range of applied field strengths. Similarly, at a fixed applied field strength $E_a^0 = 5 \times 10^5\,\text{V/m}$, the threshold frequency of the applied field to align cells for *S. oneidensis* and *B. subtilis* is lower than that for *P. aeruginosa* and *L. lactis*. Figure S2 in the Supplementary Materials summarized the threshold values of applied field strength and frequency as a function of the aspect ratio of bacteria. The figure shows that a smaller value of E_a^0 (or f) could align cells with a larger aspect ratio. We will discuss this point more later. Similar argument can be applied to understand the observations that *L. lactis* has the highest threshold value for both string and columnar phases, as it has the smallest aspect ratio among the tested strains.

In comparison of Fig. 3(a) with Fig. 3(c), although they have a similar aspect ratio, *B. subtilis* seems to be more challenging to assemble into columnar structures than *S. oneidensis*, as at the same frequency *S. oneidensis* can form columnar structures at a lower field strength than *B. subtilis*. This result suggests that there will be other factors that can contribute to the assembled structures. Then, we measured the zeta potentials of the two strains, and the results (see Fig. S3 in the Supplementary Materials) show that *B. subtilis* has a zeta potential of $-52.7\,\text{mV}$, which is more negative than that of *S. oneidensis* ($-16.1\,\text{mV}$). Cells with more negative zeta potential will have a stronger coulomb repulsion, which can make them hard to form columnar structures in *B. subtilis*. This is also supported by Supplementary Movie S1, where it shows that *B. subtilis* cells tend to form separate string-like structures during assembly process. Interestingly, among the four strains, we found that some *P. aeruginosa* cells can swim in deionized water and the ratio of swimming to non-swimming bacteria is $\sim 1.8:1$, which provides us an opportunity to investigate the effect of bacterial swimming on their directed assembly in AC electric fields. Figure S4 in the Supplementary Materials demonstrates a time series of microscopic images of *P. aeruginosa* in different applied electric fields. The flagellum of each cell was stained so it can be observed using fluorescence microscopy. We can see that when E_a^0 reaches $2 \times 10^5\,\text{V/m}$, non-swimming cells become aligned with the field while swimming bacteria can still move freely. As E_a^0 increases to $4 \times 10^5\,\text{V/m}$, the motile bacteria begin to swim along the electric field (i.e., swimming cells also become aligned). If E_a^0 increases further, cells form string-like ($1 \times 10^6\,\text{V/m}$) and columnar ($2 \times 10^6\,\text{V/m}$) structures, in which the flagellum of each cell is located either on the sides of strings or within the interstices between neighboring cells in columns. Within the string or columnar structures, cells can not swim. Together, these results suggest that the swimming mobility (or the driving power provided by rotation of flagellum) of cells increased the threshold value of electric field to align cells and when the electric field is strong enough, cell swimming is suppressed as cells are packed in string or columnar structures. However, the effect of electric field on bacterial swimming is reversible, as E_a^0 after was reduced back to $5 \times 10^5\,\text{V/m}$, cells from disassembled string or columnar structures can swim along the electric field again.

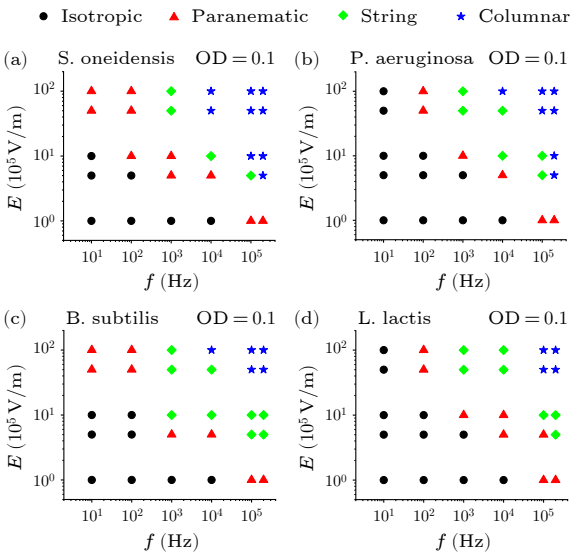

Fig. 3. Phase diagrams of dilute bacterial suspensions ($OD_{600} = 0.1$) in the plane of field strength vs field frequency for *S. oneidensis* (a), *P. aeruginosa* (b), *B. subtilis* (c), and *L. lactis* (d).

To further understand the dependence of field-mediated self-assembly of bacterial cells on cell population density, we then studied the assembled structures of

four strains in AC electric fields at $OD_{600} = 1.0$. The results are shown in Figs. 4 and 5. Figure 4 displays microscopic images of typical phases observed in concentrated suspensions and their corresponding fast Fourier transforms (FFT). We can see that by increasing the applied field strength at a fixed $f = 1\,\text{kHz}$, *S. oneidensis* cells first transit from an isotropic phase to a paranematic phase, and then enter into a higher ordered phase with interdigitating rectangular crystal domains (OIR). A schematic configuration of the crystal domain is also shown in Fig. 4. The ordered OIR phase is supported by its FFT pattern that exhibits four bright spots in a rectangle pattern. Interestingly, the distances between these four spots vary with E_a^0 (or f) increasing (see Fig. S5 in the Supplementary Materials). We summarized the measured size of rectangles consisting of the four spots at different E_a^0 (or f) in Table S1. The results show that the distance between the two spots along short-edge fluctuate, while that between those along long-edge increases as E_a^0 (or f) increases, suggesting that the OIR structure shrinks along $\boldsymbol{E}$ direction with E_a^0 (or f) increasing. In an example showing the self-assembly process of the dilute bacterial suspension (Supplementary Movie S2), it is observed that bacteria not only aggregate but also twist during this process, leading to the formation of three-dimensional rectangular domains in the concentrated bacterial suspension. These domains are characterized by each bacterium being surrounded by eight neighboring cells, with four cells aligned at each pole (as shown in Supplementary Movie S3). The entire process is schematically illustrated in Fig. S6 in the Supplementary Materials. *P. aeruginosa* cells at high density show a similar phase behavior except that the ordered phase at high field strengths is not OIR but an ordered phase with smectic A liquid crystal domains (OSA) (see the configuration selected by the corresponding red dashed box). However, compared with OIR, the OSA domain was only observed in cell monolayer regions, and the FFT of OSA does not show clearly characteristic spots of smectic A, probably because the domains of smectic A liquid crystal are too small. As demonstrated in Fig. 2, the staggered-like configurations in *S. oneidensis* and zig-zag-like configurations in *P. aeruginosa* account for a considerable fraction in assembled string structures in diluted suspensions ($OD_{600} = 0.1$). Then, at high cell densities, we can imagine that these structural units would get together to form OIR and OSA structures. For *L. lactis* cells, since they naturally exist in the form of chains with varying number of composing cells, they behave differently from *P. aeruginosa* cells even they exhibit a similar proportion of zig-zag-like units as that of *P. aeruginosa* in diluted suspensions. In the naturally formed chains of *L. lactis* cells, cells are physically connected with each other, which make the natural formed chains behaving as long rods. However, the varying length of these chains leads to a high polydispersity ($\sim 16\%$, Fig. S7 in the Supplementary Materials) of long rods, which can inhibit crystal formation, similar to the reported polydispersity effect of hard spheres, where hard sphere crystallization is suppressed when polydispersity is beyond 12%.[33,34] Additionally, *L. lactis* cells do not form columnar structures either, because along the field direction the chaining cannot be lasted continuously over the length of the field of view. Thus, at high field strengths only sheets of chains are observed. Different from the other three bacterial strains, *B. subtilis* show similar phase behavior in concentrated suspensions as in dilute ones under the same applied fields. We can see that in the columnar phase, *B. subtilis* cells form serval bundles but these bundles do not merge together even in the applied field with a strength of $10^6\,\text{V/m}$ and a frequency of 200 kHz (Fig. 4). This is probably caused by the large zeta potential of *B. subtilis*, which induces strong repulsion between strings or columnar structures to push them away from each other.

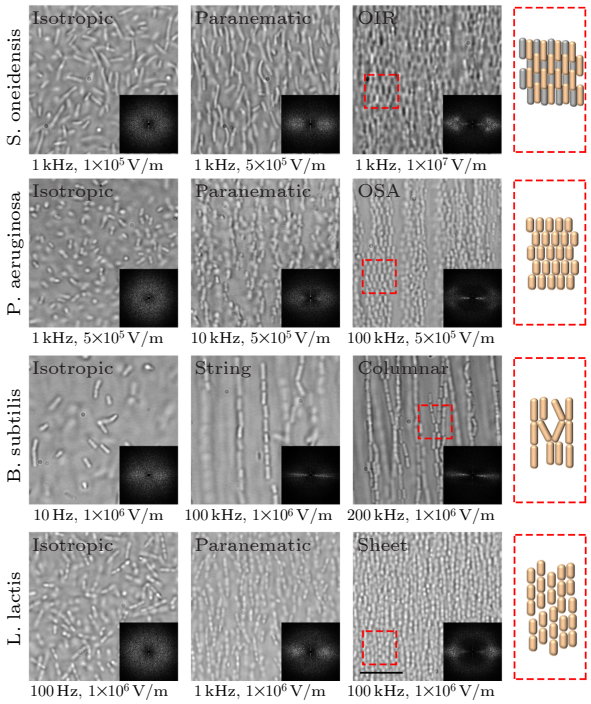

Fig. 4. Microscopic images illustrating assembled structures of relatively concentrated bacterial suspensions ($OD_{600} = 1.0$) in AC electric fields. Insets in the lower corner of images are FFTs. The cartoons of the last column are schematic representations of the corresponding configurations indicated by red dashed rectangular boxes in the images of the third column. Scale bar: 10 μm.

Figure 5 summarized the phase diagrams of four strains in relatively concentrated suspensions. Compared with the phase diagrams in diluted suspensions (Fig. 3), *S. oneidensis* and *P. aeruginosa* cells in concentrated suspensions can be condensed more by attractions between strings and/or columnar structures, so that higher ordered phases with certain crystal domains could be formed. Nevertheless, *B. subtilis* cells do not form large bundles of columnar structures in the tested range of applied electric fields, thus they have a similar phase diagram as in diluted suspensions. *L. lactis* cells are special in that they exist in a form of chains with different lengths in suspensions, and thus when being more concentrated in electric fields, they do not form

discernable columnar configurations as clear as in the case of diluted suspensions but rather tend to form sheets of chains.

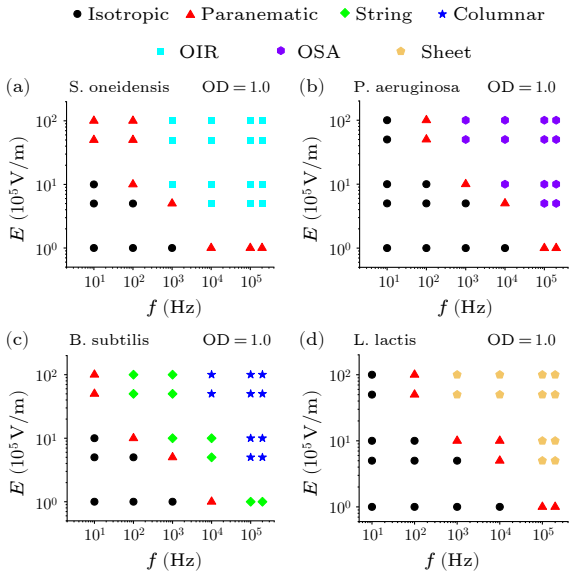

Fig. 5. Phase diagrams of concentrated suspensions (OD_{600} = 1.0) in the plane of field strength vs frequency for *S. oneidensis* (a), *P. aeruginosa* (b), *B. subtilis* (c), and *L. lactis* (d).

Discussions. In a bacterial suspension, bacterial cells have different dielectric constant from surrounding liquid environment. Thus, in an AC electric field, polarizable cells can have induced dipole moment, which then align cells with the field and also induce dipole-dipole interactions between cells. For an ideal uniformly polarized rod, ignoring variations in the polarization strength and direction inside the rod as well as any polarization due to the electric field resulting from neighboring rods, its induced dipole moment in the electric field $\boldsymbol{E}$ is given by [13,35]

$$\boldsymbol{p} = 3v_{\rm rod}\varepsilon_{\rm m}\varepsilon_0 {\rm Re}\left[\frac{\varepsilon^*_{\rm rod}-\varepsilon^*_{\rm m}}{\varepsilon^*_{\rm rod}+2\varepsilon^*_{\rm m}}\right]\boldsymbol{E}, \tag{2}$$

where $v_{\rm rod}$ is the volume of the rod, ε_0 is the vacuum permittivity, $\varepsilon_{\rm m}$ is the relative permittivity of the suspending medium, Re means to take the real part within the square brackets, and $\varepsilon^*_{\rm rod}$ and $\varepsilon^*_{\rm m}$ are complex permittivities of rod and medium, defined by $\varepsilon^*_{\rm rod} = \varepsilon_{\rm rod}\varepsilon_0 - i\frac{\sigma_{\rm rod}}{\omega}$ and $\varepsilon^*_{\rm m} = \varepsilon_{\rm m}\varepsilon_0 - i\frac{\sigma_{\rm m}}{\omega}$, respectively, with $\sigma_{\rm rod}$ and $\sigma_{\rm m}$ being conductivities of rod and medium. Thus, the induced dipole moment is affected by the permittivity and conductivity of both particles and medium, as well as the frequency of applied field. Besides these dipole-based interactions, in this study, the electric field employed is not uniform. As shown in Fig. 1, the electric field has a strong gradient near the edges of electrodes, and a low gradient at the center of the gap. Then, cells will also experience a dielectrophoretic force, [36] which will move cells from large field gradient locations (e.g., edges of electrodes) to low field gradient locations (e.g., the center of gap) or inverse depending on the sign of ${\rm Re}[\frac{\varepsilon^*_{\rm rod}-\varepsilon^*_{\rm m}}{\varepsilon^*_{\rm rod}+2\varepsilon^*_{\rm m}}]$. Under the conditions tested in this work, cells are found to move toward the gap center (i.e., low field gradient locations). Such dielectrophoretic forces also provide a way to concentrate cells at the gap center between two electrodes.

As free ions are present in bacterial suspensions, which increase the conductivity of both medium and cells, they play critical roles in the self-assembly behavior of cells based on Eq. (2). When the frequency of applied field is low, the double layers around bacterial cells can follow the electric field to be polarized and partially screen the field effect, which then reduced the actual field strength on cells. The polarized double layer was also reported to induce several phase transitions in fd-virus systems when the frequency is lower than a few kHz. [19,22] By contrast, when the frequency of applied field is high, the double layers can not respond promptly to keep up with the field frequency so that cells will experience a less-screened (hence larger) electric field. This can explain why cells in this study tend to form aligned structures even the applied field strength was kept same when the field frequency increases.

Different bacterial species can vary in cell properties including cell structures, cell morphology and cell surface properties. For example, gram-negative species *S. oneidensis* and *P. aeruginosa* have two cell membranes for each cell while gram-positive species *Bacillus subtilis* and *Lactococcus lactis* have only one cell membrane. [37] They are all rod-shape but differ in aspect ratios. In addition, the cell surface charges are also different among the four strains. Based on Eq. (2), these factors will all contribute to the permittivity and conductivity of cells, and thus can affect the self-assembly behavior of cells in the AC electric fields. Let us focus on the shapes of these bacteria. Based on our measurements, the widths of all four strains employed in this work are similar (0.6–0.85 μm). Then, a larger aspect ratio (i.e., a longer length) corresponds to a larger volume, which leads to a greater dipole moment. This is supported by our observations that a lower value of $E^0_{\rm a}$ (or f) is needed to align bacterial cells with a higher aspect ratio (*S. oneidensis* and *B. subtilis* in our case). Our results clearly show that among these factors, the aspect ratio is more important in determining the threshold value of field strength for cell alignment. However, for the assembled structures, the differences in cell morphology and cell charges can all play important roles, which lead to discernable differences in the details of structures even they belong to the same type of structures (for example, differences in string structures in Fig. 2). This is true for both diluted and concentrated suspensions.

Further understanding of the observed assembly behavior of different strains will require a more realistic modeling of bacterial cells in AC electric fields. However, bacterial cells are complex. They contain subcellular structures such as cell membranes, cell wall, and cellular substances inside cytoplasm. Their surface properties can also vary greatly by having varied compositions of proteins, polysaccharides, and other membrane associated biopolymers. [38] Equally importantly, bacterial cell properties are dynamic and can change with the environment.

All these complexities make the modeling of bacterial cells in AC electric fields a very challenging task and certainly beyond the scope of this study.

In summary, we have studied the self-assembly of four different bacterial strains in AC electric fields in both diluted and concentrated suspensions. Their phase diagrams in the plane of applied field strength vs frequency are obtained. In diluted suspensions, all four strains exhibit a transition sequence of isotropic–paranematic–string–columnar phases as the field strength increases through either the applied voltage or frequency of electric signals. However, different strains lead to different details in the assembled string and columnar structures, which has been quantitatively characterized by angle θ. In the string structures, more than 95% *B. subtilis* cells assemble into near-perfect linear unit ($\theta = 0°$–$5°$), while for *P. aeruginosa* and *L. lactis*, the cell percentage of near-perfect linear unit is down to $\sim$78% but the cell percentage of zig-zag-like unit rises to $\sim$18% ($\theta = 10°$–$15°$). For *S. oneidensis*, the cell percentage of zig-zag unit and staggered-like unit ($\theta = 15°$–$20°$) rises to $\sim$30% and $\sim$20%, respectively, at the expense of reducing the percentage of near-perfect linear unit to $\sim$40%. In concentrated suspensions, besides the isotropic and paranematic phases, higher ordered phases, i.e., OIR and OSA, are observed for *S. oneidensis* and *P. aeruginosa*, respectively. The obtained phase diagrams of four different bacterial species clearly demonstrate that bacterial cell properties including cell morphology and cell surface charges can greatly affect the assembly behavior of cells in AC electric fields. Particularly, cell aspect ratio play an important role in determining the threshold value of field strength to align cells while cell surface properties are important for understanding the details of assembled structures. In addition, our results also illustrate that cell motility can affect the threshold value of cell alignment. These results shed new light on understanding how different bacterial species may self-assemble differently in AC electric fields, which would be useful for better fabrication of biomaterials.

Acknowledgements. This work was supported by the National Key R&D Program of China (Grant No. 2023YFC3402401), and the National Natural Science Foundation of China (Grant No. 12374206).

References

[1] Li Z, Fan Q, and Yin Y 2022 *Chem. Rev.* **122** 4976
[2] Cai Z Y, Li Z W, Ravaine S *et al.* 2021 *Chem. Soc. Rev.* **50** 5898
[3] Qi F L, Meng Z H, Xue M *et al.* 2020 *Anal. Chim. Acta* **1123** 91
[4] Probst P T, Mayer M, Gupta V *et al.* 2021 *Nat. Mater.* **20** 1024
[5] Gao Y F, Ge K Y, Zhang Z *et al.* 2024 *Adv. Sci.* **11** 2305876
[6] Li C, Li Q, Kaneti Y V *et al.* 2020 *Chem. Soc. Rev.* **49** 4681
[7] Zhou A, Qiao L Y, Wei G N *et al.* 2020 *Chin. Phys. Lett.* **37** 050501
[8] Yakovlev E V, Komarov K A, Zaytsev K I *et al.* 2017 *Sci. Rep.* **7** 13727
[9] van Blaaderen A, Dijkstra M, van Roij R *et al.* 2013 *Eur. Phys. J. Spec. Top.* **222** 2895
[10] Bao M M, Igwe I E, Chen K *et al.* 2022 *Chin. Phys. Lett.* **39** 108702
[11] Snezhko A and Aranson I S 2011 *Nat. Mater.* **10** 698
[12] Erb R M, Son H S, Samanta B *et al.* 2009 *Nature* **457** 999
[13] Troppenz T, Filion L, Van Roij R *et al.* 2014 *J. Chem. Phys.* **141** 154903
[14] Kuijk A, Troppenz T, Filion L *et al.* 2014 *Soft Matter* **10** 6249
[15] Singh J P, Lele P P, Nettesheim F *et al.* 2009 *Phys. Rev. E* **79** 050401
[16] van Dommelen R, Fanzio P, and Sasso L 2018 *Adv. Colloid Interface Sci.* **251** 97
[17] Bates M A and Frenkel D 1998 *J. Chem. Phys.* **109** 6193
[18] Gupta S, Alargova R G, Kilpatrick P K *et al.* 2010 *Langmuir* **26** 3441
[19] Kang K and Dhont J K G 2008 *Europhys. Lett.* **84** 14005
[20] Siebman C, Velev O D, and Slaveykova V I 2015 *Biosensors* **5** 319
[21] Wang S, Lim S, Tasmim S *et al.* 2024 *Adv. Mater.* **36** 2309818
[22] Kang K and Dhont J K G 2010 *Soft Matter* **6** 273
[23] Samantaray K, Bhol P, Sahoo B *et al.* 2017 *ACS Omega* **2** 1019
[24] Sakimoto K K, Liu C, Lim J *et al.* 2014 *Nano Lett.* **14** 5471
[25] Mushenheim P C, Trivedi R R, Tuson H H *et al.* 2014 *Soft Matter* **10** 88
[26] Samantaray K, Mishra S R, Purohit G *et al.* 2020 *ACS Omega* **5** 5881
[27] Zhang J, Caiyin Q, Feng W *et al.* 2016 *Sci. Rep.* **6** 27973
[28] De Anda J, Lee E Y, Lee C K *et al.* 2017 *Acs Nano* **11** 9340
[29] Zhang J C, He J, Zhai C H *et al.* 2018 *Appl. Environ. Microbiol.* **84** e00219-18
[30] Mohanty P S, Bagheri P, Nöjd S *et al.* 2015 *Phys. Rev. X* **5** 011030
[31] Yethiraj A and van Blaaderen A 2003 *Nature* **421** 513
[32] Crassous J J, Mihut A M, Wernersson E *et al.* 2014 *Nat. Commun.* **5** 5516
[33] Royall C P, Poon W C K and Weeks E R 2013 *Soft Matter* **9** 17
[34] Pusey P N 1991 *Liquids, Freezing and the Glass Transition* (Amsterdam: Elsever) p 763
[35] Pethig R 1991 *Application of AC Electrical Fields to the Manipulation and Characterisation of Cells* (Aichi: Automation in Biotechnology) p 159
[36] Pohl H A 1978 *Dielectrophoresis* (New York: Cambridge University Press)
[37] Wu S 2004 *Microbial Engineering* (Beijing: Science Press) p 25 (in Chinese)
[38] Zhou D 2011 *Microbiology Course* 3nd edn (Beijing: Higher Education Press) p 14 (in Chinese)